solids

MDPI

Article

High-Pressure Synthesis of the Iodide Carbonate $Na_5(CO_3)_2I$

Yuqing Yin [1,*], Leonid Dubrovinsky [2], Andrey Aslandukov [2,3], Alena Aslandukova [2,3], Fariia Iasmin Akbar [2,3], Wenju Zhou [3], Michael Hanfland [4], Igor A. Abrikosov [1] and Natalia Dubrovinskaia [1,3]

1 Department of Physics, Chemistry and Biology (IFM), Linköping University, SE-581 83 Linköping, Sweden
2 Bayerisches Geoinstitut, University of Bayreuth, 95440 Bayreuth, Germany
3 Material Physics and Technology at Extreme Conditions, Laboratory of Crystallography, University of Bayreuth, 95440 Bayreuth, Germany
4 European Synchrotron Radiation Facility, 38000 Grenoble, France
* Correspondence: yuqing.yin@liu.se

Abstract: Here, we present the synthesis of a novel quaternary compound, iodide carbonate $Na_5(CO_3)_2I$, at 18(1) and 25.1(5) GPa in laser-heated diamond anvil cells. Single-crystal synchrotron X-ray diffraction provides accurate structural data for $Na_5(CO_3)_2I$ and shows that the structure of the material can be described as built of INa_8 square prisms, distorted NaO_6 octahedra, and trigonal planar CO_3^{2-} units. Decompression experiments show that the novel iodide carbonate is recoverable in the N_2 atmosphere to ambient conditions. Our ab initio calculations agree well with the experimental structural data, provide the equation of state, and shed light on the chemical bonding and electronic properties of the new compound.

Keywords: iodide carbonate; high pressure; X-ray diffraction; diamond anvil cell

Citation: Yin, Y.; Dubrovinsky, L.; Aslandukov, A.; Aslandukova, A.; Akbar, F.I.; Zhou, W.; Hanfland, M.; Abrikosov, I.A.; Dubrovinskaia, N. High-Pressure Synthesis of the Iodide Carbonate $Na_5(CO_3)_2I$. *Solids* **2024**, *5*, 333–340. https://doi.org/10.3390/solids5020022

Academic Editor: Sophie Guillemet-Fritsch

Received: 23 April 2024
Revised: 19 May 2024
Accepted: 30 May 2024
Published: 18 June 2024

1. Introduction

Inorganic carbonates and alkali halides are two common classes of compounds that are ubiquitous in nature. Their high-pressure (HP) behavior has been intensively studied for decades. The HP synthesis of new carbonates enriched the list of C-O anions, including now not only the planar trigonal $[CO_3]^{2-}$ group with the sp^2-hybridized carbon, common for numerous carbonates known at ambient conditions, but also "the sp^3 carbonates" [1] and other anions (ex. $[CO_4]^{4-}$ and $[C_2O_5]^{2-}$) [2–4]. Recent HP studies on alkali halides (such as the synthesis of a series of novel compounds including $NaCl_3$, Na_2Cl_3, and Na_4Cl_5 [5,6]) provide examples of how the chemistry of materials dramatically changes under HP [7,8].

The successful synthesis of alkali metal halide carbonate compounds has rarely been reported, and, so far, only two alkali metals fluoride carbonates (K_3CO_3F and Rb_3CO_3F) can be found in the Inorganic Crystal Structure Database (ICSD) [9]. The characterization of complex (quaternary) compounds in a laser-heated diamond anvil cell (LHDAC) has been extremely difficult. However, recent developments in the methodology of experiments on the single-crystal X-ray diffraction (SCXRD) from multiphase microcrystalline samples, as well as in the data analysis, especially using the DAFi program [10] for data processing, have made possible the structural characterization of individual phases in complex mixtures in DACs.

In this study, we synthesized a novel iodide carbonate $Na_5(CO_3)_2I$ through a reaction of sodium carbonate Na_2CO_3 with iodine I_2 at 18(1) GPa and a reaction of sodium iodide containing hygroscopic water (NaI + H_2O) with carbon tetraiodide CI_4 at 25.1(5) GPa after heating the mixtures to ~2000 K in DACs. The crystal structure of $Na_5(CO_3)_2I$ was solved and refined. Our ab initio calculations support experimental observations and reveal the electronic properties and chemical bonding of the novel compound.

2. Materials and Methods

2.1. Sample Preparation

Two BX90-type screw-driven diamond anvil cells (DACs) [11] equipped with 250 μm culet diamond anvils were used. The sample chambers were formed by the pre-indenting of steel (DAC #1) and rhenium (DAC #2) gaskets to ~25 μm thickness and laser-drilling a hole of 120 μm. DAC #1 was loaded with a plate (~5 μm thick, filling the whole sample chamber) of well-dried sodium carbonate Na_2CO_3 together with a piece (~10 μm in diameter and ~5 μm thick) of solid iodine. DAC #2 was loaded with one stack of a plate of NaI (2–5 μm thick, filling the whole sample chamber) and a piece of CI_4. Although Na_2CO_3 and NaI powders were dried on a heating table at 220 °C for 48 h before loading, NaI still contained water, being very hygroscopic. The pressure was measured in situ using the first-order Raman mode of the stressed diamond anvils [12]. Double-sided laser-heating of the samples up to ~2000 K was performed in the home laboratory at the Bayerisches Geoinstitut [13]; iodine and CI_4 served as laser light absorbers.

2.2. X-ray Diffraction

Synchrotron X-ray diffraction (XRD) measurements of the compressed samples were performed at ID15b (λ = 0.4100 Å, beam size ~1.5 × 1.5 μm^2) of the EBS-ESRF in Grenoble, France. In order to determine the sample position for single-crystal X-ray diffraction data acquisition, full X-ray diffraction mapping of the pressure chamber was performed. The sample positions displaying the greatest number of single-crystal reflections belonging to the phases of interest were chosen, and step-scans of 0.5° from −36° to +36° ω were performed. CrysAlis^{Pro} software (version 43.67a) [14] was utilized for single-crystal data analysis. To calibrate the instrumental model in the CrysAlis^{Pro} software, i.e., the sample-to-detector distance, detector's origin, offsets of the goniometer angles, and inclination of both the X-ray beam and detector surface with respect to the instrument axis, we used a single crystal of orthoenstatite [$(Mg_{1.93}Fe_{0.06})(Si_{1.93}Al_{0.06})O_6$, *Pbca* space group, a = 8.8117(2) Å, b = 5.1832(10) Å, and c = 18.2391(3) Å]. The DAFi program [10] was used for the search of reflections' groups belonging to individual single-crystal domains. The crystal structures were then solved and refined using OLEX2 (version 1.5) [15] software. The crystallite sizes were estimated from X-ray maps using XDI software (version 1.0.0.210) [16]. The crystallographic information is available in below Table 1 of Section 3.1. Powder XRD patterns during the decompression experiments were obtained using in-house XRD with a high-brilliance Rigaku diffractometer (Ag Kα radiation) (λ = 0.5609 Å) equipped with Osmic focusing X-ray optics and a Bruker Apex-II CCD detector.

2.3. Density Functional Theory Calculations

First-principles calculations were performed using the framework of density functional theory (DFT), as implemented in the Vienna Ab initio Simulation Package (VASP.5.4.4) [17]. The Projector-Augmented-Wave (PAW) method [18,19] was used to expand the electronic wave functions in a plane wave basis. The Generalized Gradient Approximation (GGA) functional was used for calculating the exchange-correlation energies, as proposed by Perdew–Burke–Ernzerhof (PBE) [20]. The PAW potentials adapted from the VASP library with the following valence configurations of 3*s* for Na, 5*s*5*p* for I, 2*s*2*p* for C, and 2*s*2*p* for O were used with the Na, I, C, and O POTCARs. The plane-wave kinetic energy cutoff was set to 800 eV. We performed variable cell relaxations including lattice parameters and atomic positions on the synthesized experimental structure to optimize the atomic coordinates and the cell vectors until the total forces were smaller than 10^{-3} eV $Å^{-1}$ per atom using the conjugate-gradient (CG) algorithm. In geometry optimization, we used a Gamma-centered k-mesh of 7x7x3. To increase the accuracy of ground-state electron density and density of states (eDOS), a denser Gamma-centered k-mesh of 11x11x11 and the tetrahedron smearing method with Blöchl corrections (ISMEAR = −5) were used. The crystal structure and the ELF visualization were made with VESTA software (version 3.5.7) [21]. The finite displacement method, as implemented in PHONOPY [22], was used to calculate harmonic

phonon frequencies and phonon band structures. A supercell size of 2 × 2 × 2 was used with a k-mesh size of 2 × 2 × 2 for the harmonic phonon calculations at 0 K.

3. Results

3.1. Crystal Structure of the Iodide Carbonate $Na_5(CO_3)_2I$

The structure of iodide carbonate $Na_5(CO_3)_2I$ synthesized at 18(1) and 25.1(5) GPa has the tetragonal space group $I4_1/amd$ (#141) (Figure 1). This structure type has not been known before. Full crystallographic data and refinement details are provided in Table 1, and the CIFs are deposited at CSD 2348295 and 2348296. The lattice parameters are a = 6.4543(17) Å and c = 14.638(6) Å at 18(1) GPa. In the structure of $Na_5(CO_3)_2I$, iodine atoms are in the 4*b* Wyckoff site, Na1 and Na2 atoms are in the 4*a* and 16*f* sites, O1 and O2 atoms are in the 8*e* and 16*h* sites, and C atoms are in the 8*e* site. Each I atom is surrounded by eight Na2 atoms forming an INa_8 square prism with a height of ~3.66 Å and a basis length of ~3.26 Å at 18(1) GPa. (Figure 1). The prisms are linked through common edges forming the 3D framework, with rectangular channels running along the *a* and *b* directions (Figure 1a). Sodium Na1 atoms and CO_3 groups are located in the channels (Figure 1b). The Na1 atoms are coordinated by six O atoms (two O1 and four O2) forming a distorted octahedron. These distorted octahedra are connected to each other through oxygen atoms of planar trigonal CO_3^{2-} units (Figure 1c). At 18(1) GPa, the Na-I distance in the INa_8 square prism is 2.9436(16) Å, which is compatible with the distances in the known TlI-type sodium iodide NaI (~2.82–2.95 Å) at 31 GPa [23]). As experimental structural data of Na_2CO_3 at high pressures are absent, one could only compare the average Na-O distances in the NaO_6 octahedra of $Na_5(CO_3)_2I$ (2.150(8) Å at 18(1) GPa) with the γ-Na_2CO_3 at ambient (~2.35 Å) [24] or the $P6_3/mcm$-Na_2CO_3 at 20 GPa (~2.24 Å) from theoretical calculations [25].

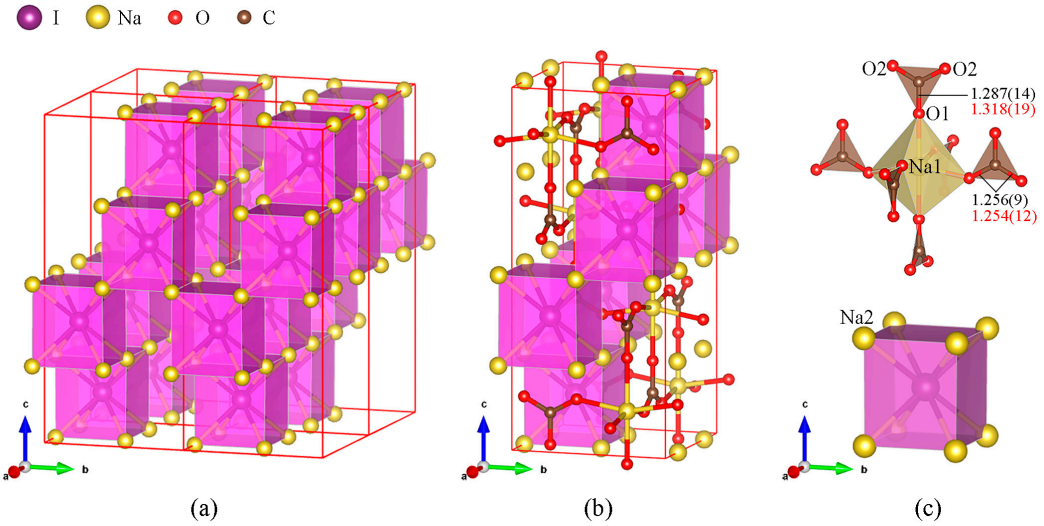

Figure 1. The structure of the novel iodide carbonate $Na_5(CO_3)_2I$ compound synthesized in this work: (**a**) 3D framework of the INa_8 cubes (carbon and oxygen atoms are not shown); (**b**) unit cell (I, Na, O, and C atoms are shown in purple, yellow, red, and brown, respectively); (**c**) building blocks of the structure: INa_8 and $Na1O_6$ polyhedra and planar CO_3 groups. The interatomic distances (in Å) in the trigonal CO_3^{2-} at 18(1) (black numbers) and 25.1(5) GPa (red numbers) are notated.

The C-O distances in the triangular CO_3^{2-} unit are different: at 18(1) GPa, the C-O1 distance is 1.287(14) Å, whereas the two C-O2 bonds are 1.256(9) Å by, that is by ~0.03 Å shorter (black numbers in Figure 1c). At 25.1(5) Gpa, the C-O1 and C-O2 are 1.318(19) and 1.254(12) Å, respectively (red numbers in Figure 1c), giving ~0.06 Å difference due to the shortening of the C-O1 bonds oriented along the *c* direction. The length of the C-O2 bond is practically unaffected. Bond angles in the CO_3^{2-} unit are slightly off from the ideal sp^2 hybridization angle of 120 degrees (O1-C-O2 vs. O2-C-O2 are 118.4(6) vs. 123.2(11) and

118.8(8) vs. 122.5(15) at 18(1) and 25.1(5) GPa, respectively). Considering this distortion, the planar trigonal CO_3^{2-} unit in $Na_5(CO_3)_2I$ does not possess the equally delocalized π-bond between C and three O atoms (unlike the CO_3^{2-} unit in γ-Na_2CO_3, whose distortion at 1 bar is insignificant; average C-O1 vs. C-O2 are 1.281(3) vs. 1.283(2) Å, giving ~0.002 Å difference [24]).

Table 1. Crystal structure, data collection, and refinement details of $Na_5(CO_3)_2I$ at 18(1) and 25.1(5) GPa in comparison to the corresponding DFT-relaxed structure.

	Crystal Data		**DFT Results**
Chemical formula	$Na_5(CO_3)_2I$	$Na_5(CO_3)_2I$	$Na_5(CO_3)_2I$
M_r	361.87	361.87	
Crystal system, space group	Tetragonal, $I4_1/amd$	Tetragonal, $I4_1/amd$	Tetragonal, $I4_1/amd$
Temperature (K)	298	298	
Pressure (GPa)	18(1)	25.1(5)	21.5
a, c (Å)	6.4543(17), 14.638(6)	6.4154(9), 14.504(4)	6.4162, 14.5214
V (Å^3)	609.8(4)	597.0(2)	597.8089
Z	4	4	
Radiation type	Synchrotron, λ = 0.4100 Å	Synchrotron, λ = 0.4100 Å	
μ (mm^{-1})	1.28	1.31	
Crystal size (mm)	0.003 × 0.003 × 0.003	0.003 × 0.003 × 0.003	
	Data Collection		
Absorption correction	Multi-scan	Multi-scan	
No. of measured, independent, and observed [$I > 2\sigma(I)$] reflections	757, 253, 215	458, 268, 192	
R_{int}	0.046	0.033	
$(\sin\theta/\lambda)_{max}$ (Å^{-1})	0.713	0.885	
	Refinement		
$R[F^2 > 2\sigma(F^2)]$, $wR(F^2)$, S	0.050, 0.130, 1.07	0.073, 0.195, 0.98	
No. of reflections	253	268	
No. of parameters	24	24	
$\Delta\rho_{max}$, $\Delta\rho_{min}$ (e Å^{-3})	1.33, −1.69	2.98, −1.90	
	Crystal Structure		
Wyckoff site, fractional atomic coordinates (x y z)	I1: 4*b*, (0 1/4 3/8) Na1: 4*a*, (0 3/4 1/8) Na2: 16*f*, (0.2448(4) 0 0) O1: 8*e*, (0 1/4 0.0213(5)) O2: 16*h*, (0 0.0788(10) 0.1500(4)) C1: 8*e*, (0 1/4 0.1092(8))	I1: 4*b*, (0 1/4 3/8) Na1: 4*a*, (0 3/4 1/8) Na2: 16*f*, (0.2454(6) 0 0) O1: 8*e*, (0 1/4 0.0184(8)) O2: 16*h*, (0 0.0787(14) 0.1509(6)) C1: 8*e*, (0 1/4 0.1093(10))	I1: 4*b*, (0 1/4 3/8) Na1: 4*a*, (0 3/4 1/8) Na2: 16*f*, (0.2430 0 0) O1: 8*e*, (0 1/4 0.0203) O2: 16*h*, (0 0.0758 0.1517) C1: 8*e*, (0 1/4 0.1093)
U_{iso} (Å^2)	I1: 0.0189(4) Na1: 0.0156(13) Na2: 0.0199(9) O1: 0.0192(16) O2: 0.0219(11) C1: 0.0139(19)	I1: 0.0163(5) Na1: 0.0169(18) Na2: 0.0172(11) O1: 0.017(2) O2: 0.0184(15) C1: 0.011(2)	

3.2. Stability and Decompression Behavior of $Na_5(CO_3)_2I$

The DFT calculations reproduced the crystal structure of the $Na_5(CO_3)_2I$ compound in good agreement with the experiment (Table 1). The formation enthalpy (ΔH) was calculated via the synthesis route of NaI + $2Na_2CO_3$ → $Na_5(CO_3)_2I$. The values of ΔH are equal to −0.217 eV/f.u. at 20 GPa (B1-type NaI [23] and the theoretically predicted $P6_3/mcm$-Na_2CO_3 [25] were adopted) and 0.130 eV/f.u. at 1 bar (average structure of the γ-Na_2CO_3 [24] and B1-type NaI were adopted). The latter value corresponds to 26 meV/atom, which is well below the "standard" 70 meV/atom limit for metastability [26]. Calcu-

lated phonon modes of $Na_5(CO_3)_2I$ revealed that the compound is dynamically stable both at the experimental volume of ~597 Å^3 (corresponding to theoretical pressure of ~21.5 GPa) (Figure 2a) and at 1 bar (Figure 2b). These results indicate that $Na_5(CO_3)_2I$, though metastable at 1 bar, is expected to be quenchable to ambient conditions.

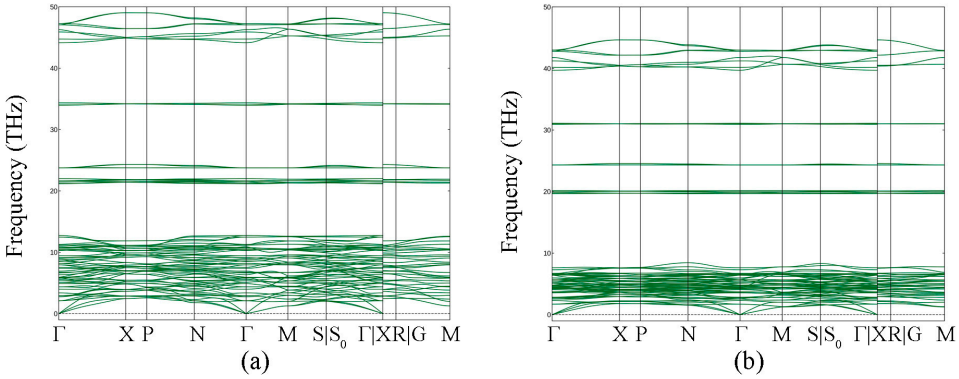

Figure 2. Phonon dispersion curves calculated at (**a**) experimental volume of ~597 Å^3, which corresponds to theoretical pressure at ~21.5 GPa, and (**b**) 1 bar along high-symmetry directions in the Brillouin zone.

DAC #1 was fully decompressed from 18(1) GPa and opened in the glove bag in an N_2 atmosphere. Then, it was closed, and the pressure after closing was 4(3) GPa. A powder XRD pattern from the recovered sample was measured in-house (see Materials and Methods). It shows that the $Na_5(CO_3)_2I$ was still preserved after the decompression (Figure 3a,b). The pressure dependence of the volume per atom for $Na_5(CO_3)_2I$ (based on the pressure–volume relations from our DFT calculations) is shown in Figure 3c along with the experimental data points. Note that the experimental data point obtained at 4(3) GPa (black circle in Figure 3c) was a result of the Le Bail fit of the powder pattern. The measured experimental volumes from SCXRD (red dots in Figure 3c) matched with the theoretical calculations, and the bulk modulus of K_0 = 43.6(3) GPa (V_0 = 13.793(9) Å^3/atom, K' = 5.10(2)) was determined from the third-order Birch–Murnaghan equation of state (3BM EOS).

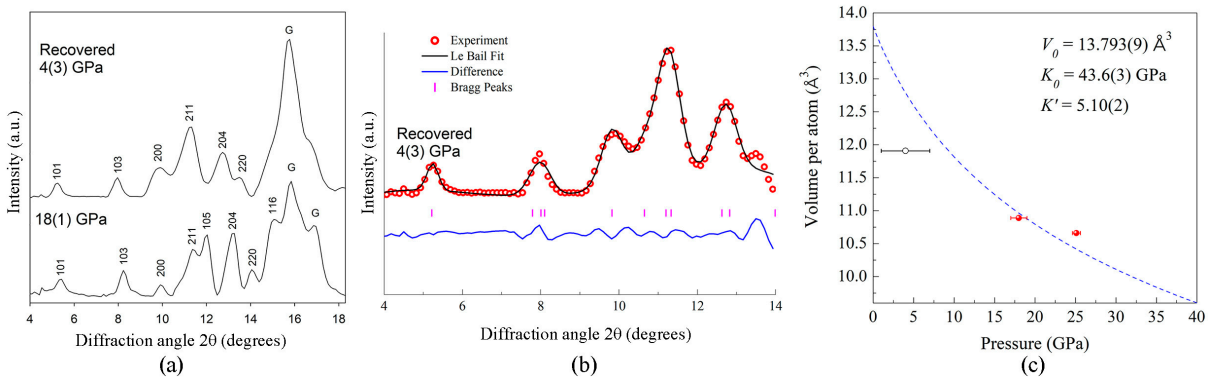

Figure 3. Some experimental and calculation data for $Na_5(CO_3)_2I$. (**a**) Powder XRD pattern collected from the recovered sample of $Na_5(CO_3)_2I$ at 4(3) GPa compared with that at the previous pressure point of 18(1) Gpa. Miller indices for $Na_5(CO_3)_2I$ are notated with black numbers; "G" refers to the gasket material. (**b**) Le Bail fit of the powder XRD pattern of $Na_5(CO_3)_2I$ at 4(3) GPa; vertical ticks correspond to Bragg peaks of $Na_5(CO_3)_2I$. X-ray wavelength λ = 0.5609Å. (**c**) The pressure dependence of the volume per atom based on the pressure–volume relations from our DFT calculations. The dashed line represents DFT-calculated volume for given pressures fitted by the 3BM EOS (V_0 = 13.793(9) Å^3/atom, K_0 = 43.6(3) GPa, K' = 5.10(2)). Black circles (powder XRD) and red dots (SCXRD) represent our experimental data points.

3.3. Electronic Properties of $Na_5(CO_3)_2I$

In order to analyze the electronic properties and chemical bonding of the $Na_5(CO_3)_2I$ compound, we performed DFT calculations of the electron localization function (ELF), band structure, and total and projected electron densities of states (TDOS and PDOS) (Figure 4).

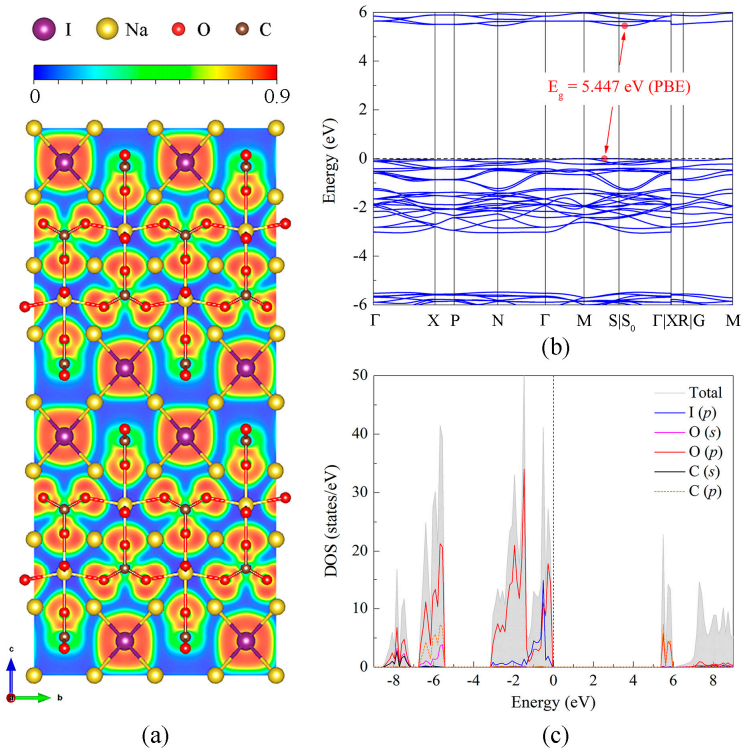

Figure 4. Calculated properties of $Na_5(CO_3)_2I$ at 21.5 GPa (experimental volume of ~597 Å^3). (**a**) ELF calculated in the (100) plane, (**b**) band structure, and (**c**) TDOS and PDOS curves of $Na_5(CO_3)_2I$. I, Na, O, and C atoms are shown in purple, yellow, red, and brown, respectively. The horizontal (in (**b**)) and vertical (in (**c**)) dashed black lines indicate the Fermi energy.

The ELF calculated in the (100) plane of the $Na_5(CO_3)_2I$ compound confirms that the I-Na2 and Na1-O interactions (Figure 1c) are closed-shell interactions (ionic), and the C-O form covalent bonds by sharing electrons (Figure 4a). The calculated band structure using the PBE GGA functional shows that $Na_5(CO_3)_2I$ has a wide bandgap of 5.447 eV at 21.5 GPa (corresponding to the experimental volume of ~597 Å^3) (Figure 4b), which means the insulator behavior of $Na_5(CO_3)_2I$. The electronic states are highly localized and the valence band maximum (VBM) occurs between **M** and **S** high symmetric points, and the conducting band minimum (CBM) is located between $\mathbf{S_0}$ and **Γ** (Figure 4b). In the eDOS of the $Na_5(CO_3)_2I$ compound, the I-5*p* and O-2*p* orbitals contribute to the highest energy of VBM, while O-2*p* and C-2*p* contribute to the lowest energy of CBM (Figure 4c), which is similar to the case of γ-Na_2CO_3 [27] (O-2*p* contribute to the highest energy of VBM and O-2*p* and C-2*p* contribute to the lowest energy of CBM). The bandgap of $Na_5(CO_3)_2I$ is relatively large if one compares it with the bandgap of γ-Na_2CO_3 (3.69 eV using PBE GGA [28], and 3.94 eV using PW91 GGA [27]), or the B1-NaI (3.9 eV using PBE GGA [29]) at 1 bar.

4. Conclusions

To summarize, we synthesized a novel iodide carbonate $Na_5(CO_3)_2I$ at 18(1) and 25.1(5) GPa. The structures were solved and refined in situ using HP synchrotron SCXRD in LHDACs. On the basis of the structural data and the results of ab initio calculations, we revealed the chemical bonding, dynamical stability, equation of state, and electronic properties of the new compound.

Author Contributions: Methodology, Y.Y., L.D., I.A.A., A.A. (Andrey Aslandukov), A.A. (Alena Aslandukova), F.I.A., W.Z. and M.H.; formal analysis, Y.Y. and L.D.; resources, L.D., I.A.A. and N.D.; writing—original draft preparation, Y.Y.; writing—review and editing, L.D., N.D., I.A.A. and A.A. (Andrey Aslandukov); supervision, L.D., N.D. and I.A.A.; funding acquisition, L.D., I.A.A. and N.D. All authors have read and agreed to the published version of the manuscript.

Funding: Y.Y. and I.A.A. acknowledge support from the Knut and Alice Wallenberg Foundation (Wallenberg Scholar grant no. KAW-2018.0194) and the Swedish Research Council (VR, grant no. 2023-05358). N.D. and L.D. thank the Deutsche Forschungsgemeinschaft (DFG projects DU 954–11/1, DU 393–9/2, DU 393–13/1, and DU 945/15-1) for financial support. N.D. and I.A.A. also thank the Swedish Government Strategic Research Area in Materials Science on Functional Materials at Linköping University (faculty grant SFO-Mat-LiU no. 2009 00971). DFT calculations were enabled by resources provided by the National Academic Infrastructure for Supercomputing in Sweden (NAISS) at the National Supercomputer Center, partially funded by the Swedish Research Council through grant agreement no. 2022-06725.

Data Availability Statement: The datasets presented in this study can be found in online repositories. The names of the repository/repositories and accession number(s) can be found below (accessed on 4 June 2024): https://www.ccdc.cam.ac.uk/structures/-, 2348295 and 2348296.

Acknowledgments: The authors acknowledge the European Synchrotron Radiation Facility (ESRF) for the provision of beamtime at the ID15b beamline. For the purpose of open access, the author has applied a Creative Commons Attribution (CC BY) license to any Author Accepted Manuscript version arising from this submission.

Conflicts of Interest: The authors declare no conflicts of interest. The funders had no role in the design of the study; in the collection, analyses, or interpretation of data; in the writing of the manuscript; or in the decision to publish the results.

References

1. Lobanov, S.S.; Dong, X.; Martirosyan, N.S.; Samtsevich, A.I.; Stevanovic, V.; Gavryushkin, P.N.; Litasov, K.D.; Greenberg, E.; Prakapenka, V.B.; Oganov, A.R.; et al. Raman spectroscopy and x-ray diffraction of sp^3 $CaCO_3$ at lower mantle pressures. *Phys. Rev. B* **2017**, *96*, 104101. [CrossRef]
2. Spahr, D.; Binck, J.; Bayarjargal, L.; Luchitskaia, R.; Morgenroth, W.; Comboni, D.; Milman, V.; Winkler, B. Tetrahedrally Coordinated sp^3-Hybridized Carbon in Sr_2CO_4 Orthocarbonate at Ambient Conditions. *Inorg. Chem.* **2021**, *60*, 5419–5422. [CrossRef] [PubMed]
3. Spahr, D.; Konig, J.; Bayarjargal, L.; Milman, V.; Perlov, A.; Liermann, H.P.; Winkler, B. $Sr[C_2O_5]$ is an Inorganic Pyrocarbonate Salt with $[C_2O_5]^{2-}$ Complex Anions. *J. Am. Chem. Soc.* **2022**, *144*, 2899–2904. [CrossRef] [PubMed]
4. Spahr, D.; Konig, J.; Bayarjargal, L.; Luchitskaia, R.; Milman, V.; Perlov, A.; Liermann, H.P.; Winkler, B. Synthesis and Structure of $Pb[C_2O_5]$: An Inorganic Pyrocarbonate Salt. *Inorg. Chem.* **2022**, *61*, 9855–9859. [CrossRef] [PubMed]
5. Yin, Y.; Aslandukova, A.; Jena, N.; Trybel, F.; Abrikosov, I.A.; Winkler, B.; Khandarkhaeva, S.; Fedotenko, T.; Bykova, E.; Laniel, D.; et al. Unraveling the Bonding Complexity of Polyhalogen Anions: High-Pressure Synthesis of Unpredicted Sodium Chlorides Na_2Cl_3 and Na_4Cl_5 and Bromide Na_4Br_5. *JACS Au* **2023**, *3*, 1634–1641. [CrossRef] [PubMed]
6. Zhang, W.; Oganov, A.R.; Goncharov, A.F.; Zhu, Q.; Boulfelfel, S.E.; Lyakhov, A.O.; Stavrou, E.; Somayazulu, M.; Prakapenka, V.B.; Konopkova, Z. Unexpected stable stoichiometries of sodium chlorides. *Science* **2013**, *342*, 1502–1505. [CrossRef] [PubMed]
7. Zhang, L.; Wang, Y.; Lv, J.; Ma, Y. Materials discovery at high pressures. *Nat. Rev. Mater.* **2017**, *2*, 17005. [CrossRef]
8. Miao, M.S.; Sun, Y.H.; Zurek, E.; Lin, H.Q. Chemistry under high pressure. *Nat. Rev. Chem.* **2020**, *4*, 508–527. [CrossRef]
9. ICSD Database. Available online: https://icsd.products.fiz-karlsruhe.de.
10. Aslandukov, A.; Aslandukov, M.; Dubrovinskaia, N.; Dubrovinsky, L. Domain Auto Finder (DAFi) program: The analysis of single-crystal X-ray diffraction data from polycrystalline samples. *J. Appl. Crystallogr.* **2022**, *55*, 1383–1391. [CrossRef]
11. Kantor, I.; Prakapenka, V.; Kantor, A.; Dera, P.; Kurnosov, A.; Sinogeikin, S.; Dubrovinskaia, N.; Dubrovinsky, L. BX90: A new diamond anvil cell design for X-ray diffraction and optical measurements. *Rev. Sci. Instrum.* **2012**, *83*, 125102. [CrossRef]
12. Akahama, Y.; Kawamura, H. Pressure calibration of diamond anvil Raman gauge to 310 GPa. *J. Appl. Phys.* **2006**, *100*, 043516. [CrossRef]
13. Fedotenko, T.; Dubrovinsky, L.; Aprilis, G.; Koemets, E.; Snigirev, A.; Snigireva, I.; Barannikov, A.; Ershov, P.; Cova, F.; Hanfland, M. Laser heating setup for diamond anvil cells for in situ synchrotron and in house high and ultra-high pressure studies. *Rev. Sci. Instrum.* **2019**, *90*, 104501. [CrossRef]
14. *Rigaku OD and CryAlis PRO*; Rigaku Oxford Diffraction Ltd.: Abingdon, UK, 2018.
15. Dolomanov, O.V.; Bourhis, L.J.; Gildea, R.J.; Howard, J.A.K.; Puschmann, H. OLEX2: A complete structure solution, refinement and analysis program. *J. Appl. Crystallogr.* **2009**, *42*, 339–341. [CrossRef]

16. Hrubiak, R.; Smith, J.S.; Shen, G. Multimode scanning X-ray diffraction microscopy for diamond anvil cell experiments. *Rev. Sci. Instrum.* **2019**, *90*, 025109. [CrossRef] [PubMed]
17. Kresse, G.; Furthmuller, J. Efficiency of ab-initio total energy calculations for metals and semiconductors using a plane-wave basis set. *Comput. Mater. Sci.* **1996**, *6*, 15–50. [CrossRef]
18. Blochl, P.E. Projector augmented-wave method. *Phys. Rev. B* **1994**, *50*, 17953–17979. [CrossRef] [PubMed]
19. Kresse, G.; Joubert, D. From ultrasoft pseudopotentials to the projector augmented-wave method. *Phys. Rev. B* **1999**, *59*, 1758–1775. [CrossRef]
20. Perdew, J.P.; Burke, K.; Ernzerhof, M. Generalized Gradient Approximation Made Simple. *Phys. Rev. Lett.* **1996**, *77*, 3865–3868. [CrossRef] [PubMed]
21. Momma, K.; Izumi, F. VESTA: A three-dimensional visualization system for electronic and structural analysis. *J. Appl. Crystallogr.* **2008**, *41*, 653–658. [CrossRef]
22. Togo, A.; Oba, F.; Tanaka, I. First-principles calculations of the ferroelastic transition between rutile-type and $CaCl_2$-type SiO_2 at high pressures. *Phys. Rev. B* **2008**, *78*, 134106. [CrossRef]
23. Léger, J.M.; Haines, J.; Danneels, C.; Oliveira, L.S.d. The TlI-type structure of the high-pressure phase of NaBr and NaI; pressure-volume behaviour to 40 GPa. *J. Phys. Condens. Matter* **1998**, *10*, 4201–4210. [CrossRef]
24. Dusek, M.; Chapuis, G.; Meyer, M.; Petricek, V. Sodium carbonate revisited. *Acta Crystallogr. B* **2003**, *59*, 337–352. [CrossRef] [PubMed]
25. Gavryushkin, P.N.; Behtenova, A.; Popov, Z.I.; Bakakin, V.V.; Likhacheva, A.Y.; Litasov, K.D.; Gavryushkin, A. Toward Analysis of Structural Changes Common for Alkaline Carbonates and Binary Compounds: Prediction of High-Pressure Structures of Li_2CO_3, Na_2CO_3, and K_2CO_3. *Cryst. Growth Des.* **2016**, *16*, 5612–5617. [CrossRef]
26. Sun, W.; Dacek, S.T.; Ong, S.P.; Hautier, G.; Jain, A.; Richards, W.D.; Gamst, A.C.; Persson, K.A.; Ceder, G. The thermodynamic scale of inorganic crystalline metastability. *Sci. Adv.* **2016**, *2*, e1600225. [CrossRef] [PubMed]
27. Duan, Y. A first-principles density functional theory study of the electronic structural and thermodynamic properties of M_2ZrO_3 and M_2CO_3 (M = Na, K) and their capabilities for CO_2 capture. *J. Renew. Sustain. Energy* **2012**, *4*, 013109. [CrossRef]
28. Cai, W.; Chen, J.; Pan, S.; Yang, Z. Enhancement of band gap and birefringence induced via π-conjugated chromophore with "tail effect". *Inorg. Chem. Front.* **2022**, *9*, 1224–1232. [CrossRef]
29. Kesek, M.; Kurt, K. First-principles calculations to investigate structural, electronic and phonon properties of sodium bromide (NaBr) and sodium iodide (NaI) crystals. *Comput. Condens. Matter.* **2022**, *31*, e00682. [CrossRef]